Atmospheric
Chemistry
and Physics
Discussions

# Exploration of PM$_{2.5}$ sources on the regional scale in the Pearl River Delta based on ME-2 modeling

Xiao-Feng Huang[1], Bei-Bing Zou[1], Ling-Yan He[1], Min Hu[2], André S. H. Prévôt[3], Yuan-Hang Zhang[2]

[1]Key Laboratory for Urban Habitat Environmental Science and Technology, School of Environment and Energy, Peking University Shenzhen Graduate School, Shenzhen, 518055, China.

[2]State Key Joint Laboratory of Environmental Simulation and Pollution Control, College of Environmental Sciences and Engineering, Peking University, Beijing, 100871, China.

[3]Paul Scherrer Institute (PSI), 5232 Villigen-PSI, Switzerland.

**Abstract:**
The Pearl River Delta (PRD) of China, which has a population of more than 58 million people, is one of the largest agglomerations of cities in the world and ever experienced severe PM$_{2.5}$ pollution at the beginning of this century. Due to the implementation of strong pollution control in recent decades, PM$_{2.5}$ in the PRD has continuously decreased to relatively lower levels in China. To comprehensively understand the current PM$_{2.5}$ sources in the PRD to support future air pollution control strategy in similar regions, we performed regional-scale PM$_{2.5}$ field observations coupled with a state-of-the-art source apportionment model at six sites in four seasons in 2015. The regional annual average PM$_{2.5}$ concentration was determined to be 37 μg/m³, which is still more than three times the WHO standard, with organic matter (36.9%) and SO$_4^{2-}$ (23.6%) as the most abundant species. A novel multilinear engine (ME-2) model was then applied to the PM$_{2.5}$ dataset in the PRD to perform source apportionment with predetermined constraints, which produced more environmentally meaningful results compared to those obtained using traditional positive matrix factorization (PMF) modeling. The regional annual average PM$_{2.5}$ source structure was retrieved to be secondary sulfate (21%), vehicle emissions (14%), industrial emissions (13%), secondary nitrate (11%), biomass burning(11%), secondary organic aerosol (SOA, 7%), coal burning (6%), fugitive dust (5%), ship emissions (3%) and aged sea salt (2%). Analyzing the spatial distribution of PM$_{2.5}$ sources under different weather conditions clearly identified the central PRD area as the key emission area for SO$_2$, NOx, coal burning, biomass burning, industrial emissions and vehicle emissions. It was further estimated that under the polluted northerly air flow in winter, local emissions in the central PRD area accounted for approximately 45% of the total PM$_{2.5}$, with secondary nitrate and biomass burning being most abundant; in contrast, the regional transport from outside the PRD accounted for more than half of PM$_{2.5}$, with secondary sulfate representing the most abundant transported species.

**Keywords:** source apportionment; ME-2; local emissions; regional transport; Pearl River Delta.

---

*Correspondence to*: L.-Y. He (hely@pku.edu.cn).

## 1 Introduction

With China's rapid economic growth and urbanization, air pollution has become a serious problem in recent decades. Due to its smaller size, fine particulate matter ($PM_{2.5}$) can carry toxic chemicals into human lungs and bronchi, causing respiratory diseases and cardiovascular diseases that can harm human health (Sarnat et al., 2008; Burnett et al., 2014). In particular, long-term exposure to high concentrations of fine particulate matter can also lead to premature death (Lelieveld et al., 2015). The Chinese government has attached great importance to improving air quality and issued the "Air Pollution Prevention and Control Action Plan" in September 2013, clearly requiring the concentrations levels of fine particulate matter in a few key regions, including the Pearl River Delta (PRD), to drop by 2017 from 15 to 25% of their values in 2012. The Pearl River Delta is one of the fastest-growing regions in China and the largest urban agglomeration in the world; it includes Guangzhou, Shenzhen, Zhuhai, Dongguan, Foshan, Huizhou, Zhongshan, Zhaoqing and Jiangmen provinces and contains more than 58 million people. The $PM_{2.5}$ concentration in this region reached a high level of 58 μg/m³ in 2007 (Nanfang Daily, 2016); however, the air quality has significantly improved due to the implementation of strict air pollution control measures, which occurred here earlier than in other regions in China. The annual average concentration of $PM_{2.5}$ in the PRD dropped to 34 μg/m³ in 2015 (Ministry of Environmental Protection, 2016).

In recent years, the receptor model method (commonly, positive matrix factorization) in the PRD was applied to perform the source apportionment of $PM_{2.5}$, which was carried out in several major cities, including Guangzhou (Gao et al., 2013; Liu et al., 2014; Wang et al., 2016), Shenzhen (Huang et al., 2014b), Dongguan (Wang et al., 2015b; Zou et al., 2017) and Foshan (Tan et al., 2016). However, the above source apportionment studies only focused on part of $PM_{2.5}$ (e.g., organic matter) or lacked the extensive representation of the PRD. Since the lifetime of $PM_{2.5}$ in the surface layer of the atmosphere is days to weeks and the cities in PRD are closely linked, the transport of $PM_{2.5}$ between cities should be specifically noteworthy (Hagler et al., 2006). On the other hand, although the positive matrix factorization (PMF) model has been successfully applied to source apportionment in the PRD, the apportionment with PMF has high rotational ambiguity and can output non-meaningful or mixed factors. Under such conditions, the multilinear engine (ME-2) model can guide the rotation toward a more objective optimal solution by utilizing a priori information (i.e., predetermined factor profiles). In recent years, ME-2, initiated and controlled via the Source Finder (SoFi) written by the Paul Scherrer Institute, was successfully developed to apportion the sources of organic aerosols (Canonaco et al., 2013). The novel ME-2 model has become a widely used and successful source analysis technique (e.g. Crippa et al., 2014; Fröhlich et al., 2015; Visser et al., 2015; Elser et al., 2016; Reyes-Villegas et al., 2016).

Accurately understanding the regional characteristics of $PM_{2.5}$ sources in the PRD can certainly guide the regional joint prevention and control of $PM_{2.5}$ in this region and provide useful references for future air pollution control strategies in China. Thus, in this study, the $PM_{2.5}$ mass and chemical compositions were measured during four seasons in 2015 at six sites in the PRD, which basically represent the pollution level of the PRD on a regional scale rather than on a city scale. The novel ME-2 model via the SoFi was applied to identify the sources of $PM_{2.5}$ in the PRD; then, the spatial locations of the sources were systematically explored using the analysis of weather conditions.
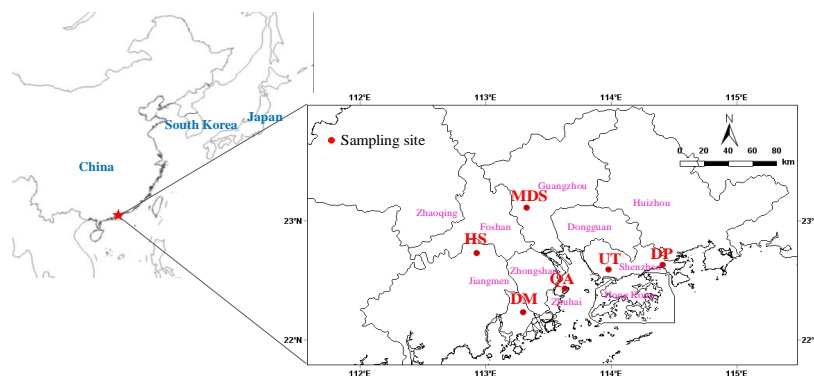
Atmospheric
Chemistry
and Physics
Discussions

## 2 Experimental methodology

### 2.1 Sampling and chemical analysis

The PRD is located in south central Guangdong Province. Based on the layout of the cities in the PRD, six sampling sites were selected to represent urban, suburban, and background sites. Detailed descriptions of these sampling sites are listed in Table 1, and their locations are shown on the regional map in Fig. 1.

**Table 1.** Description of the sampling sites in the PRD.

| Site | Site code | Coordinates | Site description | |
|------|-----------|-------------|------------------|---|
| Doumen | DM | Lat: N 22.23 | Suburban | Contains industrial areas |
| | | Lon: E 113.30 | | |
| Qi-Ao island | QA | Lat: N 22.43 | Background | An area for eco-tourism |
| | | Lon: E 113.63 | | |
| Heshan | HS | Lat: N 22.73 | Suburban | Contains industrial areas and farmlands |
| | | Lon: E 112.93 | | |
| Modiesha | MDS | Lat: N 23.11 | Urban | Contains dense urban traffic |
| | | Lon: E 113.33 | | |
| University Town | UT | Lat: N 22.59 | Urban | Contains urban traffic |
| | | Lon: E 113.98 | | |
| Dapeng | DP | Lat: N 22.63 | Background | An area for eco-tourism |
| | | Lon: E 114.41 | | |



**Fig. 1.** Spatial distribution of the sampling sites in the PRD.

Samples were collected every other day during the months of January—February (winter), April (spring), July (summer) and October—November (fall) in 2015. Each sampling period lasted for 24 h at each site. The sampling sites of University Town (UT) and Dapeng (DP) used Thermo 2300 $PM_{2.5}$ samplers (Thermo Fisher Scientific Inc., Waltham, Massachusetts, USA, with a flowrate of 16.7 L/min for two channels and a flowrate of 10.0 L/min for the other two channels), while those in Modiesha (MDS), Heshan (HS), Qi-Ao Island (QA) and Doumen (DM) used TH-16A $PM_{2.5}$ samplers (Tianhong Corp., Wu Han, China, with a flow rate of 16.7 L/min for four

100    channels). Prior to the sampling campaigns, two different types of samplers sampled in parallel

101    yielded a relative deviation of less than 5% for $PM_{2.5}$ mass concentrations. The $PM_{2.5}$ mass can be

102    obtained based on the difference in the weight of the Teflon filter before and after sampling in a

103    cleanroom at conditions of 20℃ and 50% relative humidity. Teflon filters were analyzed for their

104    major ion contents ($SO_4^{2-}$, $NO_3^-$, $NH_4^+$ and $Cl^-$) via an ion chromatography system (ICS-2500,

105    Dionex; Sunnyvale, California, USA), and their metal element contents (23 species) were

106    analyzed via an inductively coupled plasma mass spectrometer (ICP-MS, auroraM90; Bruker,

107    Germany). Quartz filters were analyzed for their organic carbon (OC) and elemental carbon (EC)

108    contents using an OC/EC analyzer (Desert Research Institute, Reno, Nevada, USA). The overall

109    organic mass (OM) was estimated as $1.8 \times OC$ (He et al., 2011).

110    The meteorological conditions during the observation period, shown in Table 2, indicated

111    that the PRD region experienced a hot and humid summer and a cool and dry winter, while spring

112    and fall were two transition seasons. Furthermore, the back trajectories of the air masses obtained

113    using the NOAA HYSPLIT model (Fig. S1) revealed that the air masses originated from the

114    northern inland in winter, from the northern inland and the South China Sea in spring, from the

115    South China Sea in summer, and from the northeast coast and the northern inland in fall.

116    **Table 2.** General meteorological conditions during the observation period in the PRD.

| | Mean Temp. (℃) | Rainfall (mm) | Mean RH (%) | Mean wind speed (m/s) | Predominant wind direction |
|---|---|---|---|---|---|
| Winter(Jan.10-Feb.9) | 17 | 35 | 63% | 2.1 | ENE |
| Spring(Apr.2-Apr.30) | 23 | 61 | 72% | 1.8 | SSW |
| Summer(Jul.1-Jul.29) | 29 | 244 | 74% | 2.1 | SW |
| Fall(Oct.11-Nov.10) | 25 | 92 | 68% | 1.7 | NNE |

117

118 **2.2 Input data matrices for source apportionment modeling**

119    PMF is a multivariate factor analysis tool widely used for aerosol source apportionment. The

120    PMF algorithm groups the measured matrix **X** (Eq. (1)) into two non-negative constant matrices **G**

121    (factor time series) and **F** (factor profiles), and **E** denotes the model residuals (Paatero and Tapper,

122    1994). The entries in **G** and **F** are fitted using a least-squares algorithm that iteratively minimizes

123    the object function $Q$ in Eq. (2), where $e_{ij}$ are the elements of the residual matrix **E**, and $u_{ij}$ are

124    the errors/uncertainties of the measured species $x_{ij}$.

125          $$\mathbf{X} = \mathbf{G} \bullet \mathbf{F} + \mathbf{E} \qquad (1)$$

126          $$Q = \sum_{i=1}^{n}\sum_{j=1}^{m}\left(e_{ij}/u_{ij}\right)^2 \qquad (2)$$

127    The multilinear engine (ME-2) was later developed by Paatero (1999) based on the PMF

128    algorithm. In contrast to an unconstrained PMF analysis, ME-2 can utilize the constraints (i.e.,

129    predetermined factor profiles) provided by the user to enhance the control of rotation for a more

130    objective solution. One or more factor profiles can be expediently input into ME-2, and the output

131    profiles are allowed to vary from the input profiles to some extent. When using ME-2 modeling,

132    the "mixed factors" can usually be better resolved.

Atmospheric
Chemistry
and Physics
Discussions

133    In this study, both PMF and ME-2 models were run for the datasets observed in the PRD. We

134    first need to determine the species input into the models. Species that may lead to high species

135    residuals or lower $R^2$ values between measured and model-predicted or non-meaning factors were

136    not included, such as those that fulfilled the following criteria: (1) species that were below

137    detection in more than 40% of samples; (2) species that yielded $R^2$ values of less than 0.4 in

138    inter-species correlation analysis; and (3) species that had little implication for pollution sources

139    and lower concentrations. Therefore, 18 species were input into the models; these species

140    accounted for 99.6% of the total measured species and included OM, EC, $SO_4^{2-}$, $NO_3^-$, $NH_4^+$, $Cl^-$,

141    K, Ca, Na, Mg, Al, Zn, Fe, Cd, V, Ni, Ti and Pb.

142    The application of PMF or ME-2 also depends on the estimated realistic uncertainty ($u_{ij}$) of

143    the individual data point of an input matrix, which determines the $Q$ value in Eq. (2). Therefore,

144    the estimation of uncertainty is an important component of the application of these models. There

145    are many sources of uncertainty, including sampling, handling, transport, storage, preparation, and

146    testing (Leiva et al., 2012). In this study, the sources of uncertainty that contributed little to the

147    total uncertainty could be neglected. Therefore, we first considered the uncertainties introduced by

148    sampling and analysis processes, such as sampling volume, repeatability analysis and ion

149    extraction. The species uncertainties $u_{ij}$ are estimated using Eq. (5), where $\bar{u}_c$ is the error

150    fraction of the species, which is estimated using the relative combined error formula Eq. (6)

151    (Vazquez et al., 2008).

152    $$u_{ij} = \bar{u}_c \times x_{ij} \qquad (5)$$

153    $$\bar{u}_c = \sqrt{\bar{u}_f^2 + \bar{u}_r^2 + \bar{u}_e^2} \qquad (6)$$

154    *where $\bar{u}_f$ is the relative error of the sampling volume; $\bar{u}_r$ is the relative error of the repeatability*

155    analysis of the standard species; and $\bar{u}_e$ is the relative error of the ion extraction of multiple

156    samples. When the concentration of the species is below the detection limit (DL), the

157    concentration values were replaced by 1/2 of DL, and the corresponding uncertainties were set at

158    5/6 of DL. Missing values were replaced by the geometric mean of the species with corresponding

159    uncertainties of 4 times their geometric mean (Polissar et al., 1998). To account for other

160    uncertainties, the estimated uncertainties ($\bar{u}_c$) of all species were further increased by a factor of 2.

161    **2.3 Constraint setup in ME-2 modeling**

162    In this study, USEPA PMF (v5.0) was first applied with the concentration matrix and

163    uncertainties matrix described above to identify the $PM_{2.5}$ sources. After examining a range of

164    factor numbers from 3 to12, the nine-factor solution output by PMF (base run, $Q_{true}/Q_{exp}=2.5$) was

165    found to be the optimal solution, since the factor of biomass burning was not extracted in the

166    eight-factor solution while the factor of fugitive dust was separated into two non-meaningful

167    factors when more factors were set to run PMF. For the nine-factor solution, the source judgement

168    based on tracers for each factor was identical to that of the ME-2 results detailed in Section 3.2.

169    However, in Fig. S2, some factors seemed to be mixed by some unexpected components and were

170    thus overestimated. For example, the secondary sulfate and secondary nitrate factors of PMF had

171    certain species from primary particulates, such as EC, Zn, Al, K and Fe, among which EC had

172    obvious EV values of 18.7% and 9.7%, respectively; the EV value of OM in the sea salt factor

173 (which was theoretically negligible) had a high value of 6.4%, and OM accounted for 37% of the

174 total mass of this factor; the EV value of $SO_4^{2-}$ in the fugitive dust factor (which was theoretically

175 negligible) had a high value of 8.6%, and the $SO_4^{2-}$ concentration accounted for 26% of the total

176 mass of this factor.

177 Therefore, using the same species concentration matrix and uncertainties matrix, we ran the

178 ME-2 model via SoFi for 9-12 factors with the four factors constrained as described above, as

179 shown in Table 3. The following considerations were used. Secondary sulfate and secondary

180 nitrate factors should theoretically not contain species from primary particulates, but they may

181 contain secondary organic matter related to the secondary conversion process of $SO_2$ and NOx (He

182 et al., 2011; Yuan et al., 2006b; Huang et al., 2014b). Therefore, the contributions of the species

183 from primary particulates were constrained to zero in the input secondary aerosol factors, while

184 others were not constrained. In addition, the factors of sea salt and fugitive dust in primary

185 aerosols could be understood based on the abundance of species in seawater and the upper crust

186 (Mason, 1982; Taylor and Mclennan, 1995). As seen in Table S1, the abundances of $Cl^-$, $Na^+$,

187 $SO_4^{2-}$, $Mg^{2+}$, $Ca^{2+}$ and $K^+$ in sea salt were relatively high, as were the abundances of Al, Fe, Ca,

188 Na, K, Mg and Ti in fugitive dust. Therefore, these high-abundance species were not constrained

189 in the sea salt and fugitive dust factors, while the other species (with abundances of less than 0.1%

190 in the particulates) were constrained to zero (Table 3). In addition, $HNO_3$ might react with sea salt

191 to displace $Cl^-$ (Huang et al., 2006); thus, $NO_3^-$ was also not constrained in the sea salt factor.

192 **Table 3.** The constraints of factor species for ME-2 modeling.

| Factors | OM | EC | Cl⁻ | NO₃⁻ | SO₄²⁻ | NH₄⁺ | Ca | Ti | V | Ni | Zn | Cd | Pb | Na | Mg | Al | K | Fe |
|---|---|---|---|---|---|---|---|---|---|---|---|---|---|---|---|---|---|---|
| Secondary sulfate | | 0 | 0 | 0 | | | 0 | 0 | 0 | 0 | 0 | 0 | 0 | 0 | 0 | 0 | 0 | 0 |
| Secondary nitrate | | 0 | 0 | | 0 | | 0 | 0 | 0 | 0 | 0 | 0 | 0 | 0 | 0 | 0 | 0 | 0 |
| Sea salt | 0 | 0 | | | | 0 | 0 | 0 | 0 | 0 | 0 | 0 | | | 0 | | 0 |
| Fugitive dust | 0 | 0 | 0 | 0 | 0 | 0 | | | 0 | 0 | 0 | 0 | 0 | | | | | |

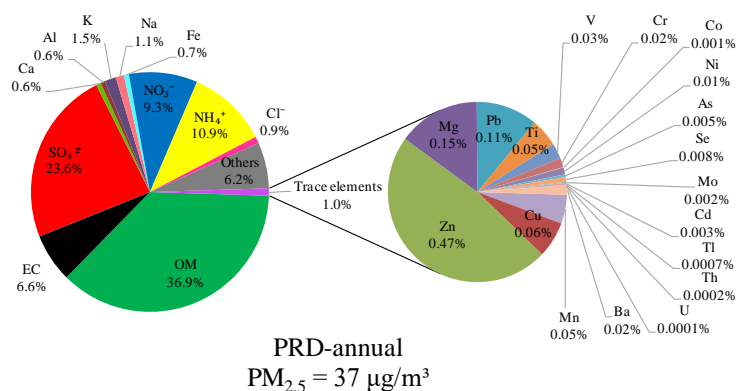193

194 **3 Results and discussion**

195 **3.1 Tempo-spatial variations of PM$_{2.5}$ in the PRD**

196 The 4-month average PM$_{2.5}$ concentration for all six sites in the PRD was 37 μg/m³, which was

197 slightly higher than the Grade II national standards for air quality (with an annual mean of 35

198 μg/m³). The chemical compositions of PM$_{2.5}$ in the PRD are shown in Fig. 2. OM had the highest

199 contribution of 36.9%, suggesting severe organic pollution in the PRD. Other important

200 components included $SO_4^{2-}$ (23.6%), $NH_4^+$ (10.9%), $NO_3^-$ (9.3%), EC (6.6%) and $Cl^-$ (0.9%).

201 The major metallic components included K (1.5%), Na (1.1%), Fe (0.7%), Al (0.6%), and Ca

202 (0.6%), and trace elements accounted for 6.2%. Fig. 3a shows the spatial distribution of the PM$_{2.5}$

203 and chemical components between six sites. The PM$_{2.5}$ pollution level in the PRD was distinctly

204 higher in the northwestern hinterland (HS and MDS) and lower in the southern coastal areas (DM

205 and DP). The much lower PM$_{2.5}$ concentration at the background DP (28 μg/m³) indicated that the

206 central PRD area was characterized by large contributions of pollution transported from outside

207 this region. At the background DP site, the fractions of $Cl^-$ and $NO_3^-$ in PM$_{2.5}$ were the lowest of

208 the six sites, i.e., 0.3% and 3.9%, respectively, suggesting that they had dominantly local sources

209 in the PRD. The highest concentration level of PM$_{2.5}$ was observed at HS (suburban), which was

210   influenced by the pollution transport of Foshan (industrial city) and Guangzhou (metropolis) under
211   the dominant northeastern wind the year. Fig. 3b shows that the seasonal variations in the major
212   components of $PM_{2.5}$ in the PRD were evidently higher in winter and lower in summer and that
213   they were correlated with monsoon characteristics. The back trajectories of the air masses (Fig. S1)
214   show that the northern monsoon prevails in winter and the southern monsoon prevails in summer
215   in the PRD. Under the northeast monsoon, the air masses mostly came from the inland and carried
216   higher concentrations of air pollutants. However, under the southwest monsoon, the air masses
217   largely originated from the South China Sea and were relatively clean. In addition, the frequent
218   rainfall and higher planetary boundary layer (PBL) in summer in the PRD also favored the
219   dispersion and removal of air pollutants (Huang et al., 2014b).

220        In 2002-2003, Hagler et al. (2006) also conducted observations and analysis of $PM_{2.5}$ in the
221   PRD and Hong Kong region, nearly 12 years before this study, as shown in Table 4. Compared
222   with Hagler's results, the $PM_{2.5}$ concentrations in this study decreased by 42% in Guangzhou
223   (MDS) and 21% in Shenzhen (UT), especially OC, EC and $SO_4^{2-}$, which decreased significantly
224   by 20%−47%, indicating that the measures taken to desulfurize coal-fired power plants, improve
225   the fuel standards of motor vehicles and phase-out yellow label vehicles have played important
226   roles in improving the air quality in the PRD region (People's Government of Guangdong
227   Province, 2012). Compared with the $PM_{2.5}$ concentrations reported by other cities in China in
228   recent years, the $PM_{2.5}$ concentrations in urban Guangzhou and Shenzhen in this study were
229   63%−75% lower than those in Beijing and Tianjin in northern China, Hainin in eastern China, and
230   Deyang in western China. However, the $PM_{2.5}$ concentrations in urban Guangzhou and Shenzhen
231   observed in this study were clearly higher than those in famous mega-cities in developed countries,
232   such as Paris, London, and Los Angeles, while they were similar to those of Santiago and Incheon.
233   It should be highlighted that the higher concentration of $SO_4^{2-}$ in the urban atmosphere of the
234   PRD is one of the major reasons leading to the higher degree of $PM_{2.5}$ pollution in the PRD
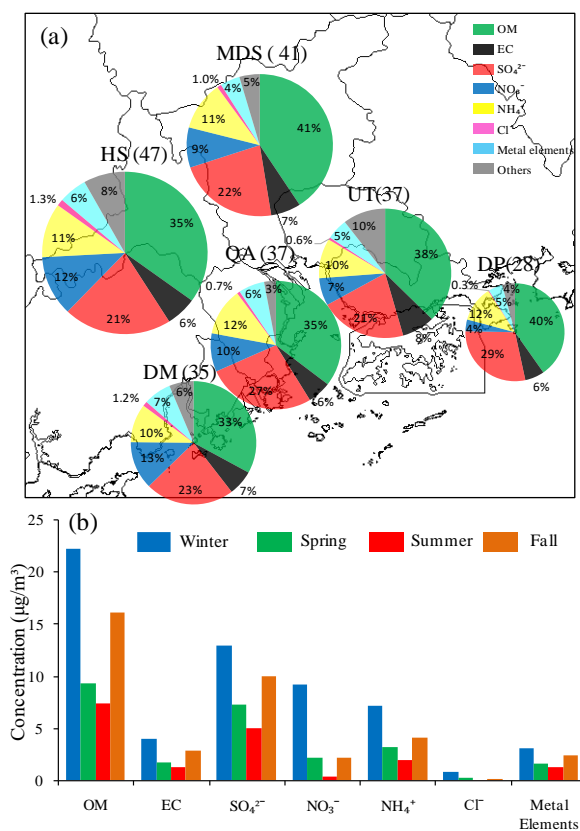235   compared to those in developed cities.



PRD-annual
$PM_{2.5} = 37\ \mu g/m^3$

236

237   **Fig. 2.** Chemical composition of annual average $PM_{2.5}$ in the PRD region.

238

Atmospheric
Chemistry
and Physics
Discussions



239

240      **Fig. 3.** The spatial distributions (a) and seasonal variations (b) of the PM$_{2.5}$ chemical compositions in the PRD

241      (unit in brackets: μg/m³).

242

243              **Table 4.** The comparison of the major chemical compositions of PM$_{2.5}$ in typical cities (unit: μg/m³).

| Cities | Periods | PM$_{2.5}$ | OC | EC | SO$_4{}^{2-}$ | NO$_3{}^-$ | NH$_4{}^+$ | References |
|---|---|---|---|---|---|---|---|---|
| Zhuhai (DM) | 2015.1–2015.11 | 35 | 6.4 | 2.3 | 8.1 | 4.4 | 3.6 | This study |
| Zhuhai (QA) | | 37 | 7.2 | 2.2 | 9.9 | 3.5 | 4.4 | |
| Jiangmen (HS) | | 47 | 9.0 | 2.8 | 9.8 | 5.6 | 5.0 | |
| Guangzhou (MDS) | | 41 | 9.3 | 2.7 | 9.2 | 3.7 | 4.6 | |
| Shenzhen (UT) | | 37 | 7.8 | 3.0 | 8.0 | 2.6 | 3.7 | |
| Shenzhen (DP) | | 28 | 6.2 | 1.8 | 8.0 | 1.1 | 3.3 | |
| Hong Kong (Urban) | 2002.10–2003.6 | 34.3 | 6.6 | 1.9 | 9.3 | 1.0 | 2.5 | Hagler et al., 2006 |
| Shenzhen (Urban) | | 47.1 | 11.1 | 3.9 | 10.0 | 2.3 | 3.2 | |
| Guangzhou (Urban) | | 70.6 | 17.6 | 4.4 | 14.7 | 4.0 | 4.5 | |
| Beijing | 2012.6–2013.4 | 112 | 17 | 6 | 24 | 20 | 16 | Wang et al., 2015a |
| Wuqing/Tianjin | 2012.11–2013.7 | 148.9 | 14.1 | 0.6 | 24.2 | 19.6 | 8.5 | Zhou et al., 2016 |
| Haining/Zhejiang | | 109.6 | 9 | 1.4 | 16.5 | 13.9 | 6.1 | |
| Deyang/Sichuan | | 121.5 | 13.8 | 1.4 | 21.6 | 10.2 | 6.3 | |
| Paris/France | 2009.9–2010.9 | 14.8 | 3.0 | 1.4 | 2.0 | 2.9 | 1.4 | Bressi et al., 2013 |

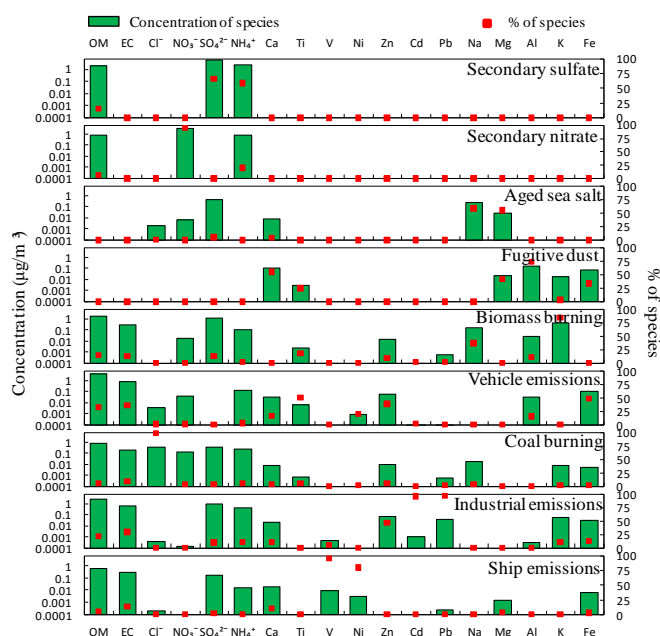| | | | | | | | |
|---|---|---|---|---|---|---|---|
| London/United Kingdom | 2003.12–2005.4 | 31.0 | 5.6 | 1.6 | 2.8 | 3.5 | 2.1 | Rodríguez et al., 2007 |
| Los Angeles/United States | 2002–2013 | 17.1 | 2.2 | 1.3 | 2.7 | 4.9 | 0.1 | Hasheminassab et al., 2014 |
| Santiago/Chile | 2013.3–2013.10 | 40 | 12.1 | 4.3 | 1.9 | 7.1 | 3.3 | Villalobos et al., 2015 |
| Incheon/Korea | 2009.6–2010.5 | 42 | 7.9 | 1.7 | 5.1 | 4.6 | 3.7 | Choi et al., 2012 |

244

245 **3.2 Source apportionment of PM$_{2.5}$ using ME-2**

246     The solutions of 9–12 factors of the ME-2 were modeled with the four factors constrained in
247 Table 3, using the SoFi tool, an implementation of ME-2 (Canonaco et al., 2013). Again, the
248 nine-factor solution provided the most reasonable source profiles, since non-interpretable factors
249 were produced (e.g., a Ti-high factor) when more factors were set to run ME-2. Based on the
250 percentage explained variations (EV) and the contributed concentrations of species in each factor
251 shown in Fig. 4, the sources of PM$_{2.5}$ can be judged as follows: (1) the first factor was explained
252 as secondary sulfate, which had large EV values of SO$_4^{2-}$ and NH$_4^+$. The high OM concentration
253 was considered to represent low-volatile oxygenated organic aerosol (LV-OOA, Jimenez et al.,
254 2009; He et al., 2011). (2) The second factor was explained as secondary nitrate, which had
255 significant EV values of NO$_3^-$ and NH$_4^+$, and its high OM concentration was considered to
256 represent semi-volatile oxygenated organic aerosol (SV-OOA, Jimenez et al., 2009; He et al.,
257 2011). (3) The third factor was related to sea salt due to the large EV values and concentrations of
258 Na and Mg. However, the low Cl$^-$ concentration and high SO$_4^{2-}$ concentration implied that SO$_4^{2-}$
259 replaced Cl$^-$ during the sea salt aging process. Therefore, this factor was identified as aged sea salt
260 (Yuan et al., 2006a). (4) The fourth factor was identified as fugitive dust due to its significant EV
261 values of Al, Ca, Mg and Fe. In this study, the undetermined mass of O and Si in this factor was
262 compensated using the elemental abundance in dust particles in Table S1 (Taylor and Mclennan,
263 1995). (5) The fifth factor was identified as biomass burning due to its significant characteristic
264 value of K (Yamasoe et al., 2000). (6) The sixth factor had high concentrations and large EV
265 values of OM and EC, as well as a certain range of EV values of Fe and Zn, which were related to
266 tires and the brake wear of motor vehicles (Yuan et al., 2006a; He et al., 2011). Therefore, this
267 factor was identified as vehicle emissions. (7) The seventh factor had a high EV value of Cl$^-$ and
268 certain concentrations of OM, EC, SO$_4^{2-}$ and NO$_3^-$, implying a combustion source. This factor
269 was identified as coal burning, which was a major source of Cl$^-$ in the PRD (Wang et al., 2015b).
270 (8) The eighth factor had large EV values of Zn, Cd and Pb, and certain concentrations of OM and
271 EC. Zn, Cd and Pb had high enrichment factors (Table S2) of 821, 4121 and 663, respectively, and
272 were thus considered to be related to industrial emissions (Wang et al., 2015b). (9) The last factor
273 had large EV values of V and Ni. V and Ni were predominantly derived from heavy oil
274 combustion, and they had high enrichment factors (Table S2) of 64 and 89, respectively. Heavy oil
275 was related to ship emissions in the PRD (Chow et al., 2002; Huang et al., 2014b). In this study,
276 secondary organic aerosol (SOA), which was not resolved as a single factor, can be extracted from
277 the factors of secondary sulfate and secondary nitrate in the forms of LV-OOA and SV-OOA,
278 respectively. Therefore, in terms of the mass balance of PM$_{2.5}$, SOA can be calculated as the sum
279 of LV-OOA and SV-OOA (Yuan et al., 2006b). It is easy to see that, in comparison with the PMF
280 modeling (Fig. S2), the ME-2 modeling indeed provided a better Q$_{true}$/Q$_{exp}$ (1.2) than the PMF
281 modeling (Q$_{true}$/Q$_{exp}$ = 2.5), and the EV values of tracers (e.g., SO$_4^{2-}$, NO$_3^-$, OM, EC, Cl$^-$, V, Ni,
282 Pb and Cd) were assigned more intensively. Therefore, it is concluded that the source
283 apportionment results of ME-2 in this study were more environmentally meaningful and

284    statistically better than those of PMF modeling.



**Fig. 4.** The factor profiles and explained variations of the ME-2 modeling.

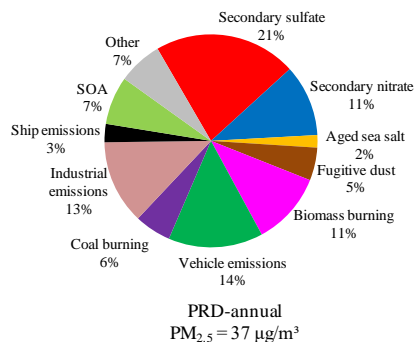287    Fig. 5 shows the 4-month average contributions of the PM$_{2.5}$ sources in the PRD in 2015
288    based on the source apportionment of ME-2. The total secondary aerosols accounted for 39% of
289    PM$_{2.5}$ in the PRD, which were secondary sulfate (21%), secondary nitrate (11%) and SOA (7%).
290    However, the identified primary particulates contributed 54% of PM$_{2.5}$, which comprised vehicle
291    emissions (14%), industrial emissions (13%), biomass burning (11%), coal burning (6%), fugitive
292    dust (5%), ship emissions (3%) and aged sea salt (2%). Unidentified sources accounted for 7%.



**Fig. 5.** The annual average contributions of PM$_{2.5}$ sources in the PRD.

**3.3 Tempo-spatial variations of sources in the PRD**

296    The spatial distributions of the PM$_{2.5}$ sources between six sites are shown in Fig. 6a.
297    Secondary sulfate represented the largest fraction (31%) of PM$_{2.5}$ at DP, indicating that it was a
298    major air pollutant in the air mass transported to the PRD. Vehicle emissions also contributed

Atmospheric
Chemistry
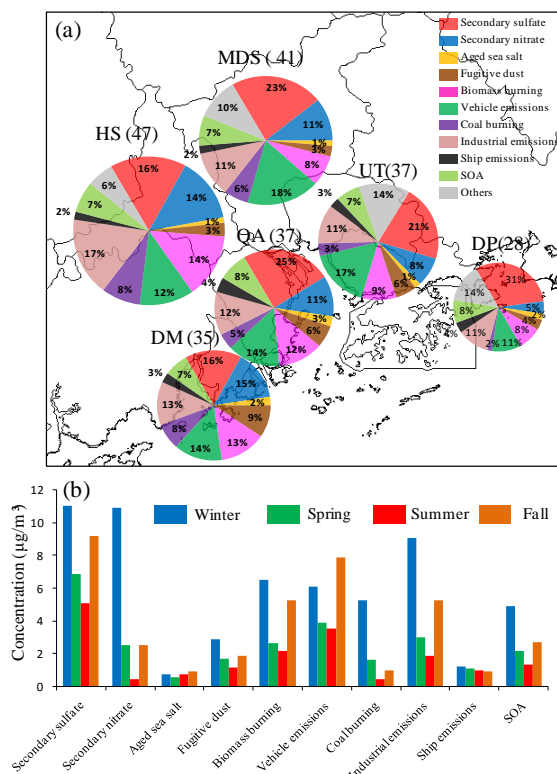and Physics
Discussions

299   relatively highly to urban sites (18% in MDS and 17% in UT). Industrial emissions, biomass
300   burning, secondary nitrate, and coal burning contributed larger fractions of $PM_{2.5}$ at HS, which
301   could be attributed to both strong local sources (e.g., the surrounding township factories and
302   farmlands) and regional transport from upwind cities at this site. Fugitive dust, which is primarily
303   related to construction activities, was relatively high at DM (9%). The contributions of ship
304   emissions and aged sea salt were the highest at QA due to its being located on Qi-Ao Island in the
305   Pearl River Estuary, which records the greatest impact from the sea. SOA contributed similar
306   amounts (7%–8%) at all sites. It should be noted that, although QA was a background site without
307   local anthropogenic sources, its $PM_{2.5}$ level was moderate in the PRD, indicating that QA was
308   impacted by severe regional transport from the surrounding cities.

309      Fig. 6b shows the seasonal variations of the major sources of $PM_{2.5}$ in the PRD. The
310   contributions of most sources were higher in winter and lower in summer, e.g., secondary sulfate,
311   secondary nitrate, fugitive dust, biomass burning, vehicle emissions, coal burning, industrial
312   emissions and SOA; these sources were correlated with monsoon characteristics and rainfall and
313   PBL variations. In contrast, the contributions of aged sea salt and ship emissions displayed little
314   seasonal variations, which could be attributed to the fact that they played more important roles
315   only when the wind came from the sea in the south, when the background levels of other air
316   pollutants were lower.

317      Previous studies of the source apportionment of bulk $PM_{2.5}$ in the PRD have mainly focused
318   on Guangzhou, Dongguan and Shenzhen, as seen in Table 5. It can be seen that in those studies,
319   $PM_{2.5}$ was apportioned to 6-9 sources and that secondary sulfate was the prominent source,
320   although the results of different studies exhibited certain differences due to the use of different
321   models or data inputs. Compared with the study of Huang et al. (2014b) in Shenzhen in 2009, the
322   contributions of secondary sulfate and vehicle emissions in Shenzhen in this study were obviously
323   lower due to power plant desulfurization and motor vehicle oil upgrades in recent years(People's
324   Government of Shenzhen Municipality, 2013). Compared with previous studies in Guangzhou,
325   this study attained more $PM_{2.5}$ sources, which can more clearly describe the source structure of
326   $PM_{2.5}$ in this region, especially industrial emissions (11%). The PRD region has experienced a
327   high degree of industrialization; thus, industrial sources should be a major source, contributing 8.1%
328   of $PM_{2.5}$ reported by the Guangzhou Environmental Protection Bureau (2017), similar to our
329   results. Tao et al. (2017) apportioned $PM_{2.5}$ to 6 sources using PMF in Guangzhou, including some
330   mixed sources. For example, ship emissions in Tao's study may not actually represent a primary
331   source due to the significant existence of some secondary inorganics and sea salt in the source
332   profile; thus, they obtained a significantly higher contribution (17%) than that in our study. Ship
333   emissions were unidentified in Huang's study (2014a) in Guangzhou.

334

335

**Fig. 6.** The spatial distributions (a) and seasonal variations (b) of PM$_{2.5}$ sources in the PRD (unit in brackets: μg/m³).

338

339

**Table 5.** Comparison of the results of source apportionment of PM$_{2.5}$ in the PRD.

| Cities | Periods | Model | Results | References |
|---|---|---|---|---|
| Guangzhou | 2015.1—2015.11 | ME-2 | Secondary sulfate (23%), secondary nitrate (11%), SOA (7%), vehicle emissions (18%), industrial emissions (11%), biomass burning (8%), coal burning (6%), fugitive dust (3%), ship emissions (2%) and aged sea salt (1%). | This study |
| Guangzhou | 2015.1—2015.2 | ME-2 | Secondary sulfate (20%), secondary nitrate (16%), SOA (8%), vehicle emissions (11%), industrial emissions (13%), biomass burning (6%), coal burning (9%), fugitive dust (2%), ship emissions (1%) and aged sea salt (1%). | This study |
| Shenzhen | 2015.1—2015.11 | ME-2 | Secondary sulfate (21%), secondary nitrate (8%) and SOA (7%), vehicle emissions (17%), industrial emissions (11%), biomass burning (9%), coal burning (3%), fugitive dust (6%), ship emissions (3%) and aged sea salt (1%). | This study |
| Guangzhou | 2014.1—2014.12 | PMF | Secondary sulfate and biomass burning (38%), ship emissions (17%), coal combustion (15%), traffic emissions (10%), secondary nitrate and chloride (12%), soil dust (7%). | Tao et al. (2017) |
| Guangzhou | 2013.1 | ME-2 | Secondary inorganic-rich (59.0%), secondary organic-rich (18.1%), traffic (8.6%), coal burning (3.4%), biomass burning (6.7%), cooking (0.8%), dust related (3.4%). | Huang et al. (2014a) |

| Dongguan | 2013.12—2014.11 | PMF | Secondary sulfate (20%), secondary nitrate (8%), SOA (10%), vehicle emissions (21%), industrial emissions (7%), biomass burning (11%), coal burning (5%), fugitive dust (8%), ship emissions (6%). | Zou et al. (2017) |
| Dongguan | 2010.2—2012.12 | PMF | Secondary sulfate (27%), secondary nitrate (19%), industrial emission (15%), biomass burning (9%) and coal combustion (9%); ship emissions/sea salt, vehicle exhaust, plastic burning and dust no more than 7%. | Wang et al. (2015b) |
| Shenzhen | 2009.1—2009.12 | PMF | Secondary sulfate (30.0%), vehicular emission (26.9%), biomass burning (9.8), secondary nitrate (9.3%), high chloride (3.8%), heavy oil combustion (3.6%), sea salt (2.6%), dust (2.5%), metallurgical industry (2.1%). | Huang et al. (2014b) |

340

**3.4 Identification of high-emission areas in the PRD in typical meteorological conditions**

341      Changes in meteorological conditions with the seasons have significant influences on the air
342 quality in the PRD (Hagler et al., 2006). The same type of weather is often repeated. Physick et al.
343 (2001) classified the weather over the region surrounding Hong Kong into seven categories based
344 on surface pressure patterns, i.e., as northerly (winter monsoon), northeasterly (winter monsoon),
345 easterly or southeasterly, trough, southerly or southwesterly (summer monsoon), cyclonic 1 and
346 cyclonic 2 weather types. The PRD region, including Hong Kong, has nearly the similar weather
347 patterns and similar meteorological conditions. In this study, the daily weather types during the
348 observation period (excluding rainy days) were also classified into seven categories based on
349 surface pressure patterns. However, according to the surface horizontal wind vectors, the PRD was
350 mostly impacted by two types of airflow, i.e., southerly flow and northerly flow. Southerly flow,
351 including the southeasterly and southerly or southwesterly (summer monsoon) weather types, was
352 relatively clean and originated from the ocean (e.g., Fig. S3 and Fig. S5). Northerly flow,
353 including the northerly (winter monsoon) and northeasterly (winter monsoon) weather types, was
354 relatively polluted and originated from the north mainland (e.g., Fig. S4 and Fig. S6). Southerly
355 flow and northerly flow appeared with the highest frequency in the PRD (i.e., above 80%). In this
356 study, southerly flow days ($PM_{2.5} \leq$ 17 µg/m³, see Table 6) were selected to better reflect the local
357 source regions in the PRD, and northerly flow days ($PM_{2.5} \geq$ 75 µg/m³, see Table 6) were selected
358 to better understand the pollution accumulation process and regional transport characteristics of
359 pollutants in the PRD. The sampling days for southerly flow and northerly flow are listed in Table
360 6.

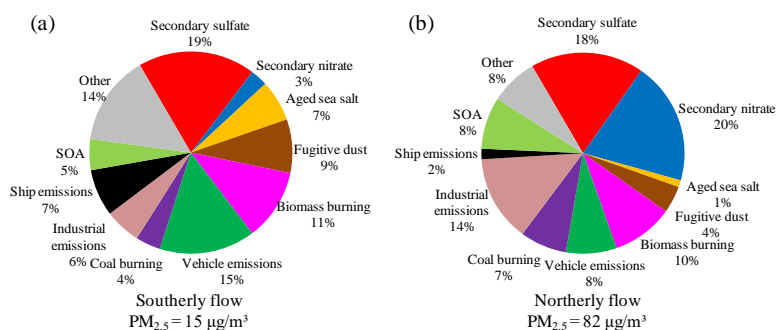**Table 6.** Sampling days categorized as southerly flow and northerly flow days.

| Southerly flow | Wind speed (m/s) | $PM_{2.5}$ (µg/m³) | Northerly flow | Wind speed (m/s) | $PM_{2.5}$ (µg/m³) |
| --- | --- | --- | --- | --- | --- |
| 2015.07.01 | 2.6 | 16 | 2015.01.18 | 2.3 | 78 |
| 2015.07.03 | 3.6 | 17 | 2015.01.20 | 1.5 | 82 |
| 2015.07.15 | 1.9 | 17 | 2015.02.03 | 2 | 75 |
| 2015.07.23 | 2.6 | 12 | 2015.02.07 | 1.7 | 101 |
| 2015.07.25 | 2 | 13 | 2015.02.09 | 2.2 | 75 |
| 2015.07.29 | 1.3 | 12 | | | |

363

364      Fig. 7 shows the contributions of $PM_{2.5}$ sources under southerly flow and northerly flow
365 conditions in the PRD. Southerly flow primarily originated from the South China Sea and carried
366 clean ocean air masses to the PRD with overall $PM_{2.5}$ values of 15 µg/m³. As shown in Fig. 7(a),
367 secondary sulfate (19%), vehicle emissions (15%) and biomass burning (11%) had higher

368  contributions under southerly flow. In contrast, in northerly flow, the level of $PM_{2.5}$ was 4.5 times
369  higher than that of southerly flow due to the transport of polluted air masses southward from the
370  north mainland. Under northerly flow, secondary sulfate (18%) and biomass burning (10%) were
371  still the major sources, but secondary nitrate became the dominant source of $PM_{2.5}$, accounting for
372  20% of $PM_{2.5}$. In addition, industrial emissions also exhibited a relatively high contribution (14%).



**Fig. 7.** Source structures of $PM_{2.5}$ in the PRD: that in southerly flow (a) and that in northerly flow (b).

376  The spatial distributions of the $PM_{2.5}$ sources under southerly flow and northerly flow are
377  shown in Fig. 8.The average concentrations of aged sea salt were similar in the summer southerly
378  flow and winter northerly flow, reflecting the local release of surrounding sea salt. Moreover, a
379  relatively high level of aged sea salt was observed at Qi-Ao Island (QA), which was consistent
380  with the geographical features of the area, which faces the sea.
381  The influences of ship emissions exhibited large differences between six sites, showing
382  significant local characteristics. The concentrations of ship emissions were the highest at DP under
383  southerly flow, mainly due to the impact of vessels in the upwind Yiantian Port, while they were
384  the highest at QA under northerly flow, primarily due to the effects of the upwind Nansha Port, as
385  shown in Fig. 9. Yantian Port and Nansha Port are among the ten largest ports in the world (Hong
386  Kong Marine Department, 2012).
387  The contributions of fugitive dust also exhibited significant differences between six sites,
388  which is consistent with local construction activities. DM is located in a newly developed zone
389  that has experienced relatively high levels of fugitive dust during southerly flow and northerly
390  flow due to active construction activities. Sample records indicate that the high value of fugitive
391  dust at UT under southerly flow maybe related to its surrounding short-term road construction
392  project, while the high value at QA under northerly flow maybe related to the operations of the
393  adjacent Nansha Port.
394  Motor vehicles are a common source of air pollution in the highly urbanized and
395  industrialized PRD region. The average concentration of vehicle emissions during northerly flow
396  was nearly 3-fold that during southerly flow. Under southerly flow, MDS, HS and UT, which are
397  located in the hinterland of the PRD, had much higher levels of vehicle emissions than the other
398  three sites; in particular, the highest level at the urban MDS site was caused by the high density of
399  motor vehicles in Guangzhou. Under northerly flow, the highest concentration of vehicle
400  emissions was still at the urban MDS site, while QA also recorded the prominent contribution of
401  vehicle emissions, which was probably closely related to the container trucks in the neighboring

Atmospheric
Chemistry
and Physics
Discussions

Open Access

402    Nansha Port. It should be noted that the concentration of vehicle emissions at the background DP
403    site exceeded half the regional average value, approaching 4 µg/m³, thus indicating that vehicle
404    emissions had a significant impact on the regional transport of air masses from the north.

405       During southerly air flow, the background DP and QA sites and the urban UT site all
406    recorded similar concentrations of secondary sulfate, suggesting that the secondary sulfate at these
407    sites was dominated by regional transport from the southern ocean with heavy vessel transport and
408    had little to do with the urban emissions at UT. Kuang et al. (2015) also found that ship emissions
409    could be a major source of secondary sulfate in the PRD in summer. HS and MDS had
410    significantly higher concentrations than their upwind site, DM, suggesting that the area between
411    MDS and HS could be a high-$SO_2$-emission area, which is consistent with the fact that this area is
412    an intensive industrial area. During northerly air flow in winter, HS and DM had lower
413    concentrations than the four upwind sites, i.e., MDS, QA, UT, and especially DP (the background
414    site), indicating that secondary sulfate could mainly be derived from regional transport from
415    outside the PRD in this season. Although the industrial area between HS and MDS could emit
416    significant amounts of $SO_2$, the lower temperatures and dry air in winter did not appear to favor
417    the quick conversion of $SO_2$ to secondary sulfate. On the other hand, the spatial distributions and
418    source characteristics of secondary sulfate also reflected the corresponding characteristics of
419    LV-OOA.

420       The spatial distributions of coal burning were significantly different between the six sites
421    during periods of both south wind and north wind, thus showing conspicuous local characteristics.
422    The contribution of coal burning was higher at MDS under southerly flow and higher at HS under
423    northerly flow. Most of the coals in the PRD were consumed by thermal power plants, but there
424    were no coal-fired power plants near the urban MDS and background DP sites. Therefore, it is
425    speculated that the high-emission areas of coal burning sources mainly exist in the region between
426    HS and MDS, as shown in Fig. 9. The distributions of coal-fired power plants in Guangdong
427    (Wang et al. 2017) reveal that some important coal-fired power plants are distributed in this region.
428    Additionally, DM also exhibited relatively obvious contributions of coal burning during southerly
429    flow and northerly flow, which is also consistent with the distribution of coal-fired power plants in
430    the vicinity.

431       The average concentration of secondary nitrate during northerly flow in winter was 40 times
432    greater than that during southerly flow in summer; this occurred not only because of the
433    unfavorable conditions of atmospheric diffusion in winter but also due to the high semi-volatility
434    of ammonium nitrate, which cannot stably exist in fine particles in the PRD during hot summer
435    (Huang et al. 2006). Under southerly flow conditions, the concentrations of secondary nitrate
436    presented prominent differences between six sites, showing local characteristics. Moreover, the
437    relatively low concentrations at the background DP site during northerly flow also indicated that
438    secondary nitrate mainly originated from the interior of the PRD. The spatial distribution
439    characteristics of secondary nitrate were very similar to those of coal burning, with the highest
440    occurring at MDS under southerly flow, the highest occurring at HS under northerly flow and
441    significantly high values occurring at DM under southerly and northerly flow, displaying that the
442    NOx emissions produced by coal burning maybe the main reason for the high nitrate levels in
443    those areas. In addition, the spatial distributions and source characteristics of secondary nitrate
444    also reflected the corresponding characteristics of LV-OOA.
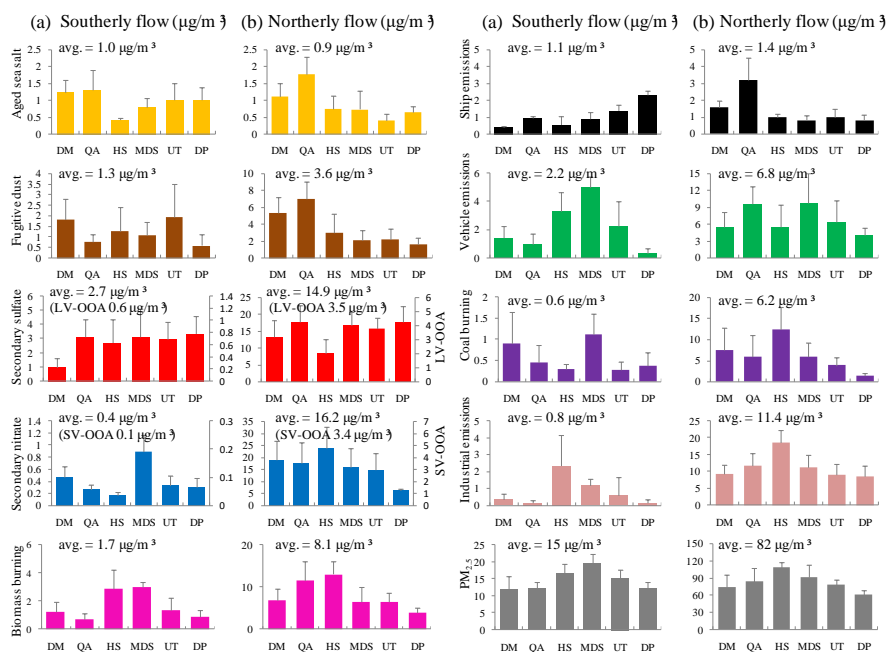
445       Under southerly flow, the influence of industrial emissions differed vastly between six sites,

446  showing obvious local characteristics. Under northerly flow, the average concentration of
447  industrial emissions reached 14-fold that of southerly flow, and the high contributions at
448  background DP suggested that regional transport probably dominated the industrial sources of fine
449  particulate matter in the PRD in winter. HS had the highest concentration of industrial emissions
450  during southerly flow and northerly flow conditions, which is consistent with the dense factories
451  present in the surrounding area (Hu, 2004; Environmental Protection Agency of Jiangmen City,
452  2017). In addition, the contribution of industrial emissions was relatively high at MDS during
453  southerly flow and relatively high at QA during northerly flow, which supports the inference that a
454  high-emission region of industrial sources was located between MDS and QA, as seen in Fig. 9.

455  The impacts of biomass burning exhibited relatively large differences between six sites
456  during both south and north wind conditions, presenting somewhat local characteristics. Suburban
457  HS had relatively high biomass burning levels during southerly flow and northerly flow, which
458  were related to the presence of more farmland in its vicinity and the frequent open-burning of crop
459  residues. The concentrations of biomass burning were relatively high at the urban MDS site during
460  southerly flow and relatively high at the background QA site during northerly flow, implying that
461  there was a high-emission area of biomass burning between MDS and QA, as shown in Fig. 9.
462  Those spatial distribution characteristics of biomass burning were similar to those of industrial
463  emissions in the PRD, suggesting that not only the combustion of open-air biomass but also the
464  use of industrial biomass-boilers could make important contributions to $PM_{2.5}$ in the PRD.

465  As a summary, the central PRD area, i.e., the middle region between MDS, HS and QA (the
466  shaded region in Fig. 9), represents the most important pollutant emissions area in the PRD; these
467  emissions include $SO_2$, NOx, coal burning, biomass burning, industrial emissions and vehicle
468  emissions, thus leading to high pollution levels in the PRD. Therefore, this area is a key area for
469  pollution control in the PRD. Primary fine particulate matter and $SO_2$ from ship emissions had
470  significant impacts on $PM_{2.5}$ in the southern coastal area of the PRD during summer southerly
471  flow, and special attention must be paid to them.

Atmospheric
Chemistry
and Physics
Discussions



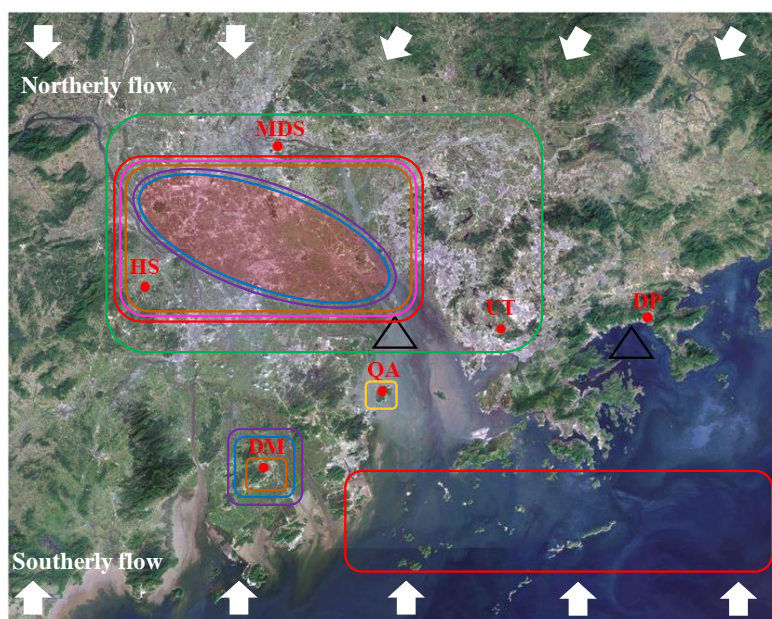**Fig. 8.** The average contributions of PM$_{2.5}$ sources at six sites in the PRD: (a) those in southerly flow, (b) those in northerly flow.



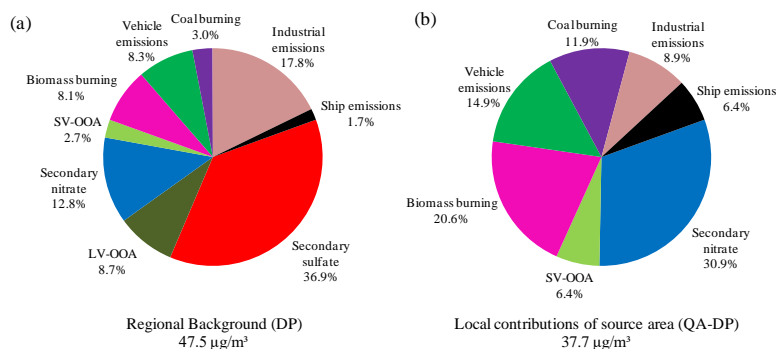**Fig. 9.** The schematic diagram of high-emission areas in the PRD (box colors correspond to those in Fig. 8, and shaded area indicates the key emission area).

Atmospheric
Chemistry
and Physics
Discussions

### 3.5 Distinguishing local and regional PM$_{2.5}$ pollution in the PRD

479

480      The analyses presented in Section 3.4 indicate that the secondary sulfates at the four southern
481 coastal sites (DM, QA, UT and DP) in the PRD were almost entirely derived from the conversion
482 of SO$_2$ from the emissions of ships in the southern ocean during southerly flow, contributing
483 approximately 20% of the average PM$_{2.5}$ (13 μg/m³) at the four sites. Considering that the ship
484 emissions directly contributed approximately 10% of the average PM$_{2.5}$ at the four sites, the total
485 ship emissions contributed approximately 30% of PM$_{2.5}$ in the southern coastal PRD area and
486 acted as the largest source of PM$_{2.5}$. Under northerly flow conditions, the background DP site,
487 which was barely affected by pollution emissions within the PRD, reflected regional transport
488 from the north air mass outside the PRD, while the background QA site reflected the superposition
489 effect of regional background pollution and the input of the most serious pollution area in the PRD.
490 The consistency of the secondary sulfate concentrations at the background QA and DP sites was
491 interpreted to reflect almost the same regional background effect during northerly flow; thus, the
492 differences in the six anthropogenic sources between the two background sites, including
493 secondary nitrate (and SV-OOA), biomass burning, industrial emissions, coal burning, vehicle
494 emissions and ship emissions, could be used to trace the internal inputs from the most serious
495 pollution area within the PRD to the downwind area. The internal inputs of six anthropogenic
496 sources to the corresponding sources of PM$_{2.5}$ at the background QA site were 66%, 67%, 28%,
497 76%, 59% and 75%, respectively, and the total internal input of 37.7 μg/m³ accounted for 45% of
498 PM$_{2.5}$ at the background QA site, showing that the local contributions of anthropogenic pollution
499 emissions in the key source area of the PRD were still crucial in winter but lower than the
500 contribution of the regional background. Ignoring natural sources, such as aged sea salt and
501 fugitive dust, under northerly flow, the contributions of other anthropogenic sources to DP were
502 considered to represent regional background pollution, and the differences in their corresponding
503 source concentrations between QA and DP were expected to represent the local emissions of
504 source areas in the PRD. Therefore, the source structures in the regional background air mass and
505 local emissions of heavy pollution sources area in the PRD are shown in Fig. 10a and b.
506 Secondary sulfate and LV-OOA occupied the vast majority (45.6%) of the regional background air
507 mass from the northern mainland, followed by industrial emissions (17.8%), secondary nitrate and
508 SV-OOA (15.5%). However, the major sources between the sources output by local emissions
509 from the heavy pollution source area of the PRD were secondary nitrate and SV-OOA (37.3%),
510 biomass burning (20.6%), vehicle emissions (14.9%) and coal burning (11.9%). Therefore,
511 measures implemented for the effective control of PM$_{2.5}$ in the PRD should focus on local controls
512 and regional joint prevention and control under winter northerly flow conditions.

513



(a)

Vehicle emissions 8.3%
Coal burning 3.0%
Industrial emissions 17.8%
Biomass burning 8.1%
SV-OOA 2.7%
Ship emissions 1.7%
Secondary nitrate 12.8%
LV-OOA 8.7%
Secondary sulfate 36.9%

Regional Background (DP) 47.5 μg/m³

(b)

Coal burning 11.9%
Industrial emissions 8.9%
Vehicle emissions 14.9%
Ship emissions 6.4%
Biomass burning 20.6%
Secondary nitrate 30.9%
SV-OOA 6.4%

Local contributions of source area (QA-DP) 37.7 μg/m³

Atmospheric
Chemistry
and Physics
Discussions

514 **Fig. 10.** The PM$_{2.5}$ source structures: (a) those in regional background air and (b) locally produced
515 pollution of the central PRD area under northerly flow.
516

517 **4 Conclusions**
518     The PRD is one of the largest agglomeration of cities in the world, and its air quality has
519 largely improved in recent decade. To reveal the current PM$_{2.5}$ pollution characteristics on a
520 regional scale in the PRD, six sampling sites were selected to conduct 4 months of sampling and
521 chemical analysis in 2015; then, the source exploration of PM$_{2.5}$ was performed using a novel
522 method. The conclusions are described below.
523 (1) The 4-month average PM$_{2.5}$ concentration for all six sites in the PRD was 37 μg/m³, of which
524 OM, SO$_4^{2-}$, NH$_4^+$, NO$_3^-$, EC, metal elements and Cl$^-$ contributed 36.9%, 23.6%, 10.9%, 9.3%,
525 6.6%, 6.5% and 0.9%, respectively. The tempo-spatial PM$_{2.5}$ variations were generally
526 characterized as being higher in the north inland region and higher in winter.
527 (2) This study revealed that theME-2 model produced more environmentally meaningful and
528 statistically robust results of source apportionment than the traditional PMF model. Secondary
529 sulfate was found to be the dominant source of PM$_{2.5}$ in the PRD, at 21%, followed by vehicle
530 emissions (14%), industrial emissions (13%), secondary nitrate (11%), biomass burning (11%),
531 SOA (7%), coal burning (6%), fugitive dust (5%), ship emissions (3%) and aged sea salt (2%).
532 Only aged sea salt and ship emissions did not show obvious seasonal variations.
533 (3) Based on the spatial distribution characteristics of PM$_{2.5}$ sources under typical southerly and
534 northerly airflow conditions, the central PRD area between MDS, HS and QA is identified as a
535 key area for source emissions, including SO$_2$, NOx, coal burning, biomass burning, industrial
536 emissions and vehicle emissions, and thus deserves more attention when implementing local
537 pollution control in the PRD. In addition, ship emissions should be controlled more strictly during
538 summer due to its contribution of approximately 30% of PM$_{2.5}$ in the southern coastal area of the
539 PRD under southerly air flow.
540 (4) Under typical winter northerly flow, the contributions of anthropogenic pollution emissions in
541 the central PRD area contributed 37.7 μg/m³ (45% of PM$_{2.5}$) to the regional background air.
542 Secondary sulfate (36.9%), industrial emissions (17.8%), and secondary nitrate SV-OOA (12.8%)
543 were the major PM$_{2.5}$ sources for the PM$_{2.5}$ transported in the regional background air mass, while
544 secondary nitrate (30.9%), biomass burning (20.6%), vehicle emissions (14.9%) and coal burning
545 (11.9%) were the major sources for the PM$_{2.5}$ produced in the central PRD area. Therefore,
546 effective control measures of PM$_{2.5}$ in the PRD in the future should pay more attention to both
547 local controls and regional joint prevention.
548

554

555 **References**
556 Bressi, M., Sciare, J., Ghersi, V., Bonnaire, N., Nicolas, J. B., Petit, J. E., Moukhtar, S., Rosso, A.,
557     Mihalopoulos, N., Féron, A.: A one-year comprehensive chemical characterisation of fine aerosol

Atmospheric
Chemistry
and Physics
Discussions

558     (PM$_{2.5}$) at urban, suburban and rural background sites in the region of Paris (France), Atmos. Chem.
559     Phys., 15, 7825-7844, doi: 10.5194/acp-13-7825-2013, 2013.

560     Burnett, R. T., Pope, C. A. I., Ezzati, M., Olives, C., Lim, S. S., Mehta, S., Shin, H. H., Singh, G.,
561     Hubbell, B., Brauer, M., Anderson, H. R., Smith, K. R., Balmes, J. R., Bruce, N. G., Kan, H., Laden,
562     F., Prüss-Ustün, A., Turner, M. C., Gapstur, S. M., Diver, W. R., and Cohen, A.: An Integrated Risk
563     Function for Estimating the Global Burden of Disease Attributable to Ambient Fine Particulate
564     Matter Exposure, Environ. Health Persp., 122, A235-A235, doi: 10.1289/ehp.122-A235, 2014.

565     Choi, J., Heo, J., Ban, S., Yi, S., Zoh, K.: Chemical characteristics of PM2.5 aerosol in Incheon, Korea.
566     Atmos. Environ., doi: 10.1016/j.atmosenv.2012.06.078, 583-592, 2012.

567     Chow, J. C., and Watson, J. G.: Review of PM2.5 and PM10 Apportionment for Fossil Fuel
568     Combustion and Other Sources by the Chemical Mass Balance Receptor Model, Energ. Fuel., 16,
569     222-260, doi: 10.1021/ef0101715, 2002.

570     Canonaco, F., Crippa, M., Slowik, J. G., Baltensperger, U., and Prévôt, A. S. H.: SoFi, an IGOR-based
571     interface for the efficient use of the generalized multilinear engine (ME-2) for the source
572     apportionment: ME-2 application to aerosol mass spectrometer data, Atmos. Meas. Tech., 6,
573     3649-3661, doi: 10.5194/amt-6-3649-2013, 2013.

574     Crippa, M., Canonaco, F., Lanz, V. A., Äijälä, M., Allan, J. D., Carbone, S., Capes, G., Ceburnis, D.,
575     Dall'Osto, M., Day, D. A., DeCarlo, P. F., Ehn, M., Eriksson, A., Freney, E., Hildebrandt Ruiz, L.,
576     Hillamo, R., Jimenez, J. L., Junninen, H., Kiendler-Scharr, A., Kortelainen, A. M., Kulmala, M.,
577     Laaksonen, A., Mensah, A. A., Mohr, C., Nemitz, E., O'Dowd, C., Ovadnevaite, J., Pandis, S. N.,
578     Petäjä, T., Poulain, L., Saarikoski, S., Sellegri, K., Swietlicki, E., Tiitta, P., Worsnop, D. R.,
579     Baltensperger, U., and Prévôt, A. S. H.: Organic aerosol components derived from 25 AMS data sets
580     across Europe using a consistent ME-2 based source apportionment approach, Atmos. Chem. Phys.,
581     14, 6159-6176, doi: 10.5194/acp-14-6159-2014 , 2014.

582     Elser, M., Huang, R., Wolf, R., Slowik, J. G., Wang, Q., Canonaco, F., Li, G., Bozzetti, C.,
583     Daellenbach, K. R., Huang, Y., Zhang, R., Li, Z., Cao, J., Baltensperger, U., El-Haddad, I., and
584     Prévôt, A. S. H.: New insights into PM$_{2.5}$ chemical composition and sources in two major cities in
585     China during extreme haze events using aerosol mass spectrometry, Atmos. Chem. Phys., 16,
586     3207-3225, doi: 10.5194/acp-16-3207-2016 , 2016.

587     Environmental Protection Agency of Jiangmen City: Key pollution sources basic information in
588     Jiangmen,     http://hbj.jiangmen.gov.cn/thirdData/hbsjzx/hjjc/fs/201712/t20171218_268676.html,
589     2017.

590     Fröhlich, R., Crenn, V., Setyan, A., Belis, C. A., Canonaco, F., Favez, O., Riffault, V., Slowik, J. G.,
591     Aas, W., Aijälä, M., Alastuey, A., Artiñano, B., Bonnaire, N., Bozzetti, C., Bressi, M., Carbone, C.,
592     Coz, E., Croteau, P. L., Cubison, M. J., Esser-Gietl, J. K., Green, D. C., Gros, V., Heikkinen, L.,
593     Herrmann, H., Jayne, J. T., Lunder, C. R., Minguillón, M. C., Močnik, G., O'Dowd, C. D.,
594     Ovadnevaite, J., Petralia, E., Poulain, L., Priestman, M., Ripoll, A., Sarda-Estève, R., Wiedensohler,
595     A., Baltensperger, U., Sciare, J., and Prévôt, A. S. H.: ACTRIS ACSM intercomparison – Part 2:
596     Intercomparison of ME-2 organic source apportionment results from 15 individual, co-located
597     aerosol mass spectrometers, Atmos. Meas. Tech., 8, 2555-2576, doi: 10.5194/amt-8-2555-2015,
598     2015.

599     Gao, B., Guo, H., Wang, X., Zhao, X., Ling, Z., Zhang, Z., and Liu, T.: Tracer-based source
600     apportionment of polycyclic aromatic hydrocarbons in PM2.5 in Guangzhou, southern China, using
601     positive matrix factorization (PMF), Environ. Sci. Pollut. R., 20, 2398-2409, doi:

602      10.1007/s11356-012-1129-0, 2013.

603    Guangzhou Environmental Protection Bureau: The Results of Source apportionment on $PM_{2.5}$ in

604      Guangzhou in 2016,

605      http://www.gz.gov.cn/gzgov/s5837/201706/1dcb25be6dd14dc6ab6506e0a5383745.shtml, 2017.

606    Hagler, G., Bergin, M., Salmon, L., Yu, J., Wan, E., Zheng, M., Zeng, L., Kiang, C., Zhang, Y., and

607      Lau, A.: Source areas and chemical composition of fine particulate matter in the Pearl River

608      region of China, Atmos. Environ., 40, 3802-3815, doi: 10.1016/j.atmosenv.2006.02.032, 2006.

609    Hasheminassab, S., Daher, N., Ostro, B. D., and Sioutas, C.: Long-term source apportionment of

610      ambient fine particulate matter (PM2.5) in the Los Angeles Basin: A focus on emissions reduction

611      from vehicular sources, Environ. Pollut., 193, 54-64, doi: 10.1016/j.envpol.2014.06.012, 2014.

612    He, L., Huang, X., Xue, L., Hu, M., Lin, Y., Zheng, J., Zhang, R., and Zhang, Y.: Submicron aerosol

613      analysis and organic source apportionment in an urban atmosphere in Pearl River Delta of China

614      using high-resolution aerosol mass spectrometry, J. Geophys. Res.-Atmos., 116, doi:

615      10.1029/2010JD014566, 2011.

616    Hong  Kong  Marine  Department:  Ranking  of  container  ports  of  the  world,

617      https://www.mardep.gov.hk/hk/publication/pdf/portstat_2_y_b5c.pdf, 2012.

618    Hu, Z. Y.: Studies on the Discharging and Distribution of Heavy Metal Pollution in the Pearl River

619      Delta, Doctoral dissertation, Graduate School of the Chinese Academy of Sciences (Guangzhou

620      Institute of Geochemistry), 2004.

621    Huang, R., Zhang, Y., Bozzetti, C., Ho, K., Cao, J., Han, Y., Daellenbach, K. R., Slowik, J. G., Platt, S.

622      M., Canonaco, F., Zotter, P., Wolf, R., Pieber, S. M., Bruns, E. A., Crippa, M., Ciarelli, G.,

623      Piazzalunga, A., Schwikowski, M., Abbaszade, G., Schnelle-Kreis, J., Zimmermann, R., An, Z.,

624      Szidat, S., Baltensperger, U., Haddad, I. E., and Prévôt, A. S. H.: High secondary aerosol

625      contribution to particulate pollution during haze events in China, Nature, 514, 218-222, doi:

626      10.1038/nature13774, 2014a.

627    Huang, X. F., Hui, Y., Gong, Z. H., Xiang, L., He, L. Y., Zhang, Y. H., and Min, H.: Source

628      apportionment and secondary organic aerosol estimation of PM2.5 in an urban atmosphere in China,

629      Sci. China Earth Sci., 57, 1352-1362, doi: 10.1007/s11430-013-4686-2, 2014b.

630    Huang, X., Yu, J. Z., He, L., and Yuan, Z.: Water-soluble organic carbon and oxalate in aerosols at a

631      coastal urban site in China: Size distribution characteristics, sources, and formation mechanisms, J.

632      Geophys. Res.-Atmos., 111, doi: 10.1029/2006JD007408, 2006.

633    Jimenez, J. L., Canagaratna, M. R., Donahue, N. M., Prevot, A. S., Zhang, Q., Kroll, J. H., Decarlo, P.

634      F., Allan, J. D., Coe, H., and Ng, N. L.: Evolution of organic aerosols in the atmosphere, Science,

635      326, 1525-1529, doi: 10.1126/science.1180353, 2009.

636    Kuang, B. Y., Lin, P., Huang, X. H. H., and Yu, J. Z.: Sources of humic-like substances in the Pearl

637      River Delta, China: positive matrix factorization analysis of PM2.5 major components and source

638      markers, Atmos. Chem. Phys., 15, 1995-2008, doi: 10.5194/acp-15-1995-2015, 2015.

639    Leiva G., M. A., Araya, M. C., Alvarado, A. M., and Seguel, R. J.: Uncertainty estimation of anions

640      and cations measured by ion chromatography in fine urban ambient particles (PM2.5), Accredit.

641      Qual. Assur., 17, 53-63, doi: 10.1007/s00769-011-0844-4, 2012.

642    Lelieveld, J., Evans, J. S., Fnais, M., Giannadaki, D., and Pozzer, A.: The contribution of outdoor air

643      pollution sources to premature mortality on a global scale, Nature, 525, 367-371, doi:

644      10.1038/nature15371, 2015.

645    Liu, J., Li, J., Zhang, Y., Liu, D., Ding, P., Shen, C., Shen, K., He, Q., Ding, X., and Wang, X.: Source

646     apportionment using radiocarbon and organic tracers for PM2.5 carbonaceous aerosols in
647     Guangzhou, South China: contrasting local- and regional-scale haze events, Environ. Sci. Technol.,
648     48, 12002, doi: 10.1021/es503102w, 2014.

649     Mason, B., Principles of Geochemistry, 2nd edition, John Wiley and Sons, 1982.

650     Ministry of Environmental Protection: Report on the State of the Environment in China 2015,
651     http://www.zhb.gov.cn/hjzl/zghjzkgb/lnzghjzkgb/201606/P020160602333160471955.pdf, 2016.

652     Nanfang Daily: $PM_{2.5}$ level fluctuations down in PRD region in the past decade,
653     http://epaper.southcn.com/nfdaily/html/2016-01-03/content_7504954.htm, 2016.

654     Paatero, P., and Tapper, U.: Positive matrix factorization: A non‐negative factor model with optimal
655     utilization of error estimates of data values, Environmetrics, 5, 111-126, doi:
656     10.1002/env.3170050203, 1994.

657     Paatero, P.: The Multilinear Engine—A Table-Driven, Least Squares Program for Solving Multilinear
658     Problems, Including the n-Way Parallel Factor Analysis Model, J. Comput. Graph. Stat., 8, 854-888,
659     doi: 10.1080/10618600.1999.10474853, 1999.

660     People's Government of Guangdong Province: Major Pollutants Emission Reduction
661     implementation plan during the 12th Five-year Plan in Guangdong Province,
662     http://zwgk.gd.gov.cn/006939748/201212/t20121219_359131.html, 2012.

663     People's Government of Shenzhen Municipality: Air quality improvement plan in Shenzhen,
664     http://zwgk.gd.gov.cn/007543382/201309/t20130930_407564.html, 2013.

665     Physick, W. L., and Goudey, R.: Estimating an annual-average RSP concentration for Hong Kong
666     using days characteristic of the dominant weather patterns, Atmos. Environ., 35, 2697-2705, doi:
667     10.1016/S1352-2310(00)00413-1, 2001.

668     Polissar, A. V., Hopke, P. K., Paatero, P., Malm, W. C., and Sisler, J. F.: Atmospheric aerosol over
669     Alaska: 2. Elemental composition and sources, J. Geophys. Res.-Atmos., 103, 19045 - 19057, 1998.

670     Reyes-Villegas, E., Green, D. C., Priestman, M., Canonaco, F., Coe, H., Prévôt, A. S. H., and Allan, J.
671     D.: Organic Aerosol source apportionment in London 2013 with ME-2: exploring the solution space
672     with annual and seasonal analysis, Atmos. Chem. Phys., 16, 15545-15559, doi:
673     10.5194/acp-16-15545-2016 , 2016.

674     Rodríguez, S., Van Dingenen, R., Putaud, J.-P., Dell'Acqua, A., Pey, J., Querol, X., Alastuey, A.,
675     Chenery, S., Ho, K.-F., Harrison, R., Tardivo, R., Scarnato, B., and Gemelli, V.: A study on the
676     relationship between mass concentrations, chemistry and number size distribution of urban fine
677     aerosols in Milan, Barcelona and London, Atmos. Chem. Phys., 7, 2217-2232, doi:
678     10.5194/acp-7-2217-2007 , 2007.

679     Sarnat, J. A., Marmur, A., Klein, M., Kim, E., Russell, A. G., Sarnat, S. E., Mulholland, J. A., Hopke, P.
680     K., and Tolbert, P. E.: Fine Particle Sources and Cardiorespiratory Morbidity: An Application of
681     Chemical Mass Balance and Factor Analytical Source-Apportionment Methods, Environ. Health
682     Persp., 116, 459-66, doi: 10.1289/ehp.10873, 2008.

683     Tan, J., Duan, J., Ma, Y., He, K., Cheng, Y., Deng, S., Huang, Y., and Si-Tu, S.: Long-term trends of
684     chemical characteristics and sources of fine particle in Foshan City, Pearl River Delta: 2008–2014,
685     Sci. Total Environ., 565, 519-528, doi: 10.1016/j.scitotenv.2016.05.059, 2016.

686     Tao, J., Zhang, L., Cao, J., Zhong, L., Chen, D., Yang, Y., Chen, D., Chen, L., Zhang, Z., Wu, Y., Xia,
687     Y., Ye, S., and Zhang, R.: Source apportionment of PM2.5 at urban and suburban areas of the Pearl
688     River Delta region, south China - With emphasis on ship emissions, Sci. Total Environ., 574,
689     1559-1570, doi: 10.1016/j.scitotenv.2016.08.175, 2017.

690  Taylor, S. R., and Mclennan, S. M.: The geochemical evolution of the continental crust, Rev. Geophys.,
691      33, 293-301, doi: 10.1029/95RG00262, 1995.

692  Vazquez, R., and Steinberg, M.: Evaluation of measurement data - Guide to the expression of
693      uncertainty in measurement, Biotechniques, 26, 2008.

694  Villalobos, A. M., Barraza, F., Jorquera, H., and Schauer, J. J.: Chemical speciation and source
695      apportionment of fine particulate matter in Santiago, Chile, 2013, Sci. Total Environ., 512-513,
696      133-142, doi: 10.1016/j.scitotenv.2015.01.006, 2015.

697  Visser, S., Slowik, J. G., Furger, M., Zotter, P., Bukowiecki, N., Canonaco, F., Flechsig, U., Appel, K.,
698      Green, D. C., Tremper, A. H., Young, D. E., Williams, P. I., Allan, J. D., Coe, H., Williams, L. R.,
699      Mohr, C., Xu, L., Ng, N. L., Nemitz, E., Barlow, J. F., Halios, C. H., Fleming, Z. L., Baltensperger,
700      U., and Prévôt, A. S. H.: Advanced source apportionment of size-resolved trace elements at multiple
701      sites  in  London  during  winter,  Atmos.  Chem.  Phys.,  15,  11291-11309,  doi:
702      10.5194/acp-15-11291-2015 , 2015.

703  Wang, H., Tian, M., Li, X., Chang, Q., Cao, J., Yang, F., Ma, Y., He, K.: Chemical Composition and
704      Light Extinction Contribution of PM2.5 in Urban Beijing for a 1-Year Period, Aerosol Air Qual.
705      Res., 15, 2200-2211, doi: 10.4209/aaqr.2015.04.0257, 2015a.

706  Wang, J., Ho, S. S. H., Ma, S., Cao, J., Dai, W., Liu, S., Shen, Z., Huang, R., Wang, G., and Han, Y.:
707      Characterization of PM2.5 in Guangzhou, China: uses of organic markers for supporting source
708      apportionment, Sci. Total Environ., 550, 961-971, doi: 10.1016/j.scitotenv.2016.01.138 , 2016.

709  Wang, Q. Q., Huang, X. H. H., Zhang, T., Zhang, Q., Feng, Y., Yuan, Z., Wu, D., Lau, A. K. H., and
710      Yu, J. Z.: Organic tracer-based source analysis of PM2.5 organic and elemental carbon: A case study
711      at  Dongguan  in  the  Pearl  River  Delta,  China,  Atmos.  Environ.,  118,  164-175,  doi:
712      10.1016/j.atmosenv.2015.07.033, 2015b.

713  Wang, Q., Feng, Y., Huang, X. H. H., Griffith, S. M., Zhang, T., Zhang, Q., Wu, D., and Yu, J. Z.: Non
714      ‐ polar organic compounds as PM2.5 source tracers: Investigation of their sources and degradation
715      in  the  Pearl  River  Delta,  China,  J.  Geophys.  Res.-Atmos.,  121,  11862-11879,  doi:
716      10.1002/2016JD025315, 2017.

717  Yamasoe, M. A., Artaxo, P., Miguel, A. H., and Allen, A. G.: Chemical composition of aerosol
718      particles from direct emissions of vegetation fires in the Amazon Basin: water-soluble species and
719      trace elements, Atmos. Environ., 34, 1641-1653, doi: 10.1016/S1352-2310(99)00329-5, 2000.

720  Yuan, Z., Lau, A., Zhang, H., Yu, J., Louie, P., and Fung, J.: Identification and spatiotemporal
721      variations of dominant PM10 sources over Hong Kong, Atmos. Environ., 40, 1803-1815, doi:
722      10.1016/j.atmosenv.2005.11.030, 2006a.

723  Yuan, Z. B., Yu, J. Z., Lau, A. K. H., Louie, P. K. K., and Fung, J. C. H.: Application of positive
724      matrix factorization in estimating aerosol secondary organic carbon in Hong Kong and its
725      relationship with secondary sulfate, Atmos. Chem. Phys., 6, 25-34, doi: 10.5194/acp-6-25-2006,
726      2006b.

727  Zhou, J., Xing, Z., Deng, J., and Du, K.: Characterizing and sourcing ambient PM2.5 over key
728      emission regions in China I: Water-soluble ions and carbonaceous fractions, Atmos. Environ., 135,
729      20-30, doi: 10.1016/j.atmosenv.2016.03.054, 2016.

730  Zou, B. B., Huang, X. F., Zhang, B., Dai, J., Zeng, L. W., Feng, N., and He, L. Y.: Source
731      apportionment of PM2.5 pollution in an industrial city in southern China, Atmos. Pollut. Res., 8,
732      1193-1202, doi: 10.1016/j.apr.2017.05.001, 2017.